Received: 29 April 2019 | Revised: 15 June 2019 | Accepted: 6 July 2019

DOI: 10.1002/chir.23115

SPECIAL ISSUE ARTICLE

WILEY

Chiral superstructures from homochiral Zn^{2+}, Co^{2+}, Fe^{2+}-2,6-bis (*aryl* ethylimine)pyridine complexes

Florina Dumitru[1,2] | Arie van der Lee[1] | Mihail Barboiu[1]

[1] Institut Européen des Membranes, UMR-CNRS 5635, Université Montpellier, ENSCM Place eugene Bataillon CC047, Montpellier, France

[2] Faculty of Applied Chemistry and Materials Science, Department of Inorganic Chemistry, Physical Chemistry and Electrochemistry, University Politehnica of Bucharest, Bucharest, Romania

Correspondence
Mihail Barboiu, Institut Européen des Membranes, UMR-CNRS 5635, Université Montpellier, ENSCM Place eugene Bataillon CC047, Montpellier, France.
Email: mihail-dumitru.barboiu@umontpellier.fr

Funding information
Agence Nationale de la Recherche, Grant/Award Number: ANR-15-CE29-0009 DYNAFUN

Abstract

We report the hierarchical supramolecular organization of metallosupramolecular homochiral complexes **1**-Λ-(S,S,S,S)-M^{2+}/**1**-Δ-(R,R,R,R)-M^{2+} and **2**-Λ-(S,S,S,S)-M^{2+}/**2**-Δ- (R,R,R,R)-M^{2+} of M^{2+} = Co^{2+}, Fe^{2+}, Zn^{2+} metal ions with chiral pseudo-terpyridine-type ligands: **1**-(S,S) or **1**-(R,R) = 2,6-*bis* (naphthyl ethylimine)pyridine and **2**-(S,S) or **2**-(R,R) = 2,6-*bis* (phenyl-ethylimine)pyridine. Circular dichroism measurements in solution were used to confirm the enantiomeric nature of all twelve complexes. For crystal structures of **1**- Λ- (S,S,S,S)-M^{2+} or **1**-Δ- (R,R,R,R)-M^{2+} complexes, absolute configurations {Δ (or P), Λ (or M)} were confirmed by refinement of the Flack parameter x: $-0.007 \leq x \leq 0.11$ for the single crystals of **1**-Λ-(S,S,S,S)-M^{2+}/**1**-Δ- (R,R,R,R)-M^{2+}, **2**- Λ- (S,S,S,S)-Fe^{2+}, and **2**-Δ- (R,R,R,R)-Co^{2+}.

KEYWORDS

aromatic interactions, chiral single crystals, imine, metallosupramolecular complexes, self-assembly

1 | INTRODUCTION

Chiral symmetry breaking and transfer of chiral information from molecular towards supramolecular level through noncovalent interactions are topics of great interest. *Molecular and supramolecular chirality* both may be used as tools to assemble systems into dissymmetric crystalline architectures based on selective chiral packing.[1] Chiral metallosupramolecular complexes are of considerable interest because of their important applications as stereodynamic probes for chiral sensing,[2-5] for the preparation of chiral catalysts,[6,7] and for the development of multifunctional materials.[8] In the design and the synthesis of chiral ligands that, upon coordination with metal ions, can induce high stereoselectivity at a supramolecular level, Schiff bases with stereogenic centres in their backbones have been extensively used as powerful tools for the spontaneous generation of chiral superstructures. Typically, these chiral Schiff bases are obtained by condensation between aldehydes and chiral primary amines, and, among the most frequently used chiral amines, one can include enantiomeric pairs of R-(+)-1-/S-(−)-1-phenylethylamine and R-(+)-1-/S-(−)-1-naphthylethylamine.[9-43]

Herein, we report six enantiomeric pairs of M^{2+} = Zn^{2+}, Co^{2+}, Fe^{2+} mononuclear complexes: **1**-Λ-(S,S,S,S)-M^{2+}/**1**-Δ-(R,R,R,R)-M^{2+} and **2**-Λ-(S,S,S,S)-M^{2+}/**2**-Δ-(R,R,R,R)-M^{2+}, where **1**-(S,S) or **1**-(R,R) are 2,6-*bis* (naphthylethylimine)pyridine and **2**-(S,S) or **2**-(R,R) = 2,6-*bis* (phenylethylimine)pyridine, Schiff bases containing two stereogenic centres. The metal ions are used to template the Schiff base formation from R-(+)-1-/S-(−)-1-phenyl-ethylamine, R-(+)-1-/S-(−)-1-naphthylethylamine, and 2,6-pyridine-dicarbox-aldehyde (Scheme 1). The resulted pseudo-terpyridines ligands orthogonally wrap around the metal ion centres, positioning their four stereogenic centres such that the metal ions are overally surrounded by chiral coordination centres, as revealed

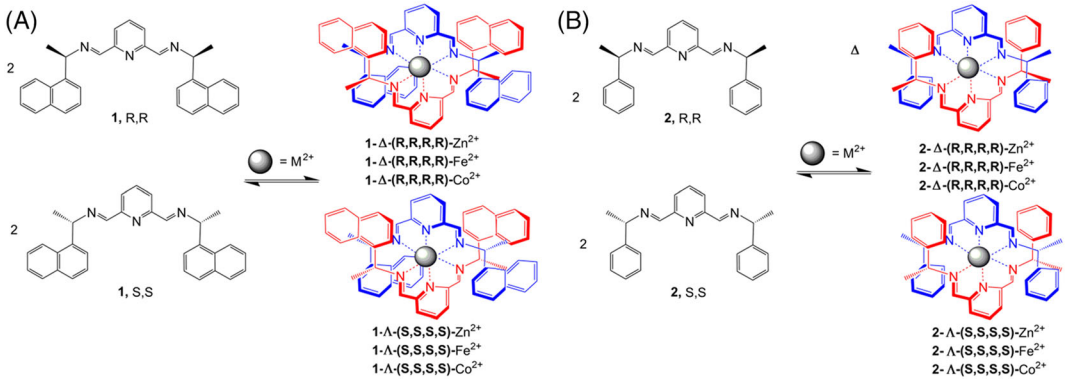

SCHEME 1 One-pot synthesis of homochiral complexes: A) **1**-Λ-(S,S,S,S)-M^{2+}/**1**-Δ-(R,R,R,R)-M^{2+} and B) **2**-Λ-(S,S,S,S)-M^{2+}/**2**-Δ-(R,R,R,R)-M^{2+}; M^{2+} = Zn^{2+}, Fe^{2+}, Co^{2+}

by X-ray crystal structures and circular dichroism (CD) spectra.

The metal ion coordination by *chiral molecular* ligands results in the formation of highly compact *chiral supramolecular* homodimers: **1**- Λ-(S,S,S,S)-M^{2+} and **1**--Δ-(R,R,R,R)-M^{2+} stabilized by strong internal π-π stacking interactions between lateral aromatic arms and central pyridine moiety. Further self-assembly in the resolved solid-state homochiral metallosupramolecular domains is observed in some cases with the formation of unique double-stranded monohelices with single handedness. The solid-phase homochirality is determined by a subtle interplay of four directional orthogonal-pseudo-terpyridine coordination geometry and "locked" by weak interactions π-π/CH⋯π interactions between peripheral aryl rings.[8,44-46]

Usually, such helical metallosupramolecular complexes crystallize in distinct alternative P and M columns or layers of Δ or Λ mirror enantiomers, but, overall, the crystals are racemic. Intermolecular crystal packing is usually not discriminating: A system of enantiomeric complexes evolves towards solid-phase homochirality if homochiral interactions between molecules are more stable than heterochiral interactions,[47] but the greater stability of homochiral versus heterochiral interactions is a necessary but not a sufficient condition for establishing solid-phase homochirality.

There are a few previous examples of direct crystallization of enantiopure helical supramolecular single crystals,[48-50] more often the crystal is racemic since homochiral layers of opposite chirality could be present and connected *via* different chirality inverting interactions. Examples of homochiral supramolecular helices were reported by us, in our previous work[51-57] on complexes of Zn^{2+}, Co^{2+}, Fe^{2+}, Pb^{2+} metal ions with *bis* (*arene* imine) pyridines ligands, but these examples are exclusively based on *achiral ligands*, and the resulted solid-state chirality is promoted by constitutional chiral affinity of supramolecular helices of the same handedness, interacting *via* their van der Waals hypersurfaces.[51a]

2 | MATERIALS AND METHODS

R-(+)-1-/S-(−)-1-phenylethylamine, R-(+)-1-/S-(−)-1-naphthylethyl-amine, 2,6-pyridinemethanol, MnO_2, Zn $(CF_3SO_3)_2$, Fe $(BF_4)_2 \cdot 6H_2O$, Co $(BF_4)_2 \cdot 6H_2O$, and CD_3CN were purchased from Aldrich and used as received. All other reagents were obtained from commercial suppliers and used without further purification. All organic solutions were routinely dried over molecular sieves 4 Å. 2,6-Pyridinedicarboxaldehyde was prepared by oxidation of 2,6-pyridinemethanol with activated MnO_2, according to the procedure described in the literature.[58]

Proton nuclear magnetic resonance (^{1}H-NMR) spectra were recorded on DRX 400 MHz Bruker Avance spectrometer, in CD_3CN, with the use of the residual solvent peak as reference. Mass spectrometric studies were performed in the positive ion mode using a quadrupole mass spectrometer (Micromass, Platform 2+). Samples were dissolved in acetonitrile and were continuously introduced into the mass spectrometer at a flow rate of 10 mL/min through a Waters 616HPLC pump. The temperature (80 °C) and the extraction cone voltage (V_c = 5-10 V) were usually set to avoid fragmentations. The notations used for the assignments of the ^{1}H-NMR signals are given below.

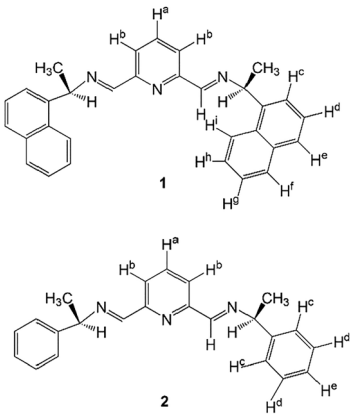

Ultraviolet-visible (UV-vis) absorbance spectra were recorded using a Kontron Instruments Uvikon 923 spectrometer, in acetonitrile 10^{-4} M to 10^{-5} M, with acetonitrile as a reference. CD spectra were measured on a Jasco J-810 spectrometer, with a DC150 W xenon lamp. Measurements were collected using a 1-mm path-length quartz cuvette, and the standard parameters used were as follows: bandwidth 2 nm, response time 1 second, wavelength scan range 190 to 600 nm, data pitch 0.2 nm, scanning speed 50 nm·min^{-1}, and accumulation 5.

2.1 | X-ray single crystal diffraction structure solution and refinement

Crystal evaluation and data collection were performed on a Rigaku Oxford-Diffraction Xcalibur-I or a Gemini-S diffractometer with sealed-tube Mo-$K\alpha$ radiation using the *CrysAlis Pro* program (Table 1).[59] The same program was used for the integration of the data using default parameters, for the empirical absorption correction using spherical harmonics employing symmetry-equivalent and redundant data, and the correction for Lorentz and polarization effects. The crystal structures were solved using the ab initio iterative charge flipping method with parameters described elsewhere[60] using the *Superflip* program,[61] and they were refined using full-matrix least-squares procedures as implemented in *CRYSTALS*[62] on all independent reflections with $I > 2\sigma(I)$. Special attention was given to the determination of the absolute structure of each compound. The compounds **1**-(R,R,R,R)-Co^{2+} and **1**-(S,S,S,S)Co^{2+} crystallize each in an enantiomorphic space group. The structure solution was therefore done in each space group of the enantiomorphic pair, and the space group was chosen on the basis of having the Flack parameter close to 0.00. The other compounds crystallize in non-enantiomorphic Sohncke space groups, and the structure was inverted if the Flack parameter was found to be close to 1.0. All final Flack and Hooft parameters[61,63-67] are very close to 0.00. Following an analysis based on maximum likelihood estimation and Bayesian statistics, the chance of having an enantiopure material is in all cases 100%.[68] The H atoms were all located in a difference map but repositioned geometrically. They were initially refined with soft restraints on the bond lengths and angles to regularize their geometry (C—H in the range 0.93-0.98 Å) and U_{iso}(H) (in the range 1.2-1.5 times U_{eq} of the parent atom), after which the positions were refined with riding constraints.[69] In some cases, thermal similarity restraints were used especially for solvent molecules. In one case, an acetonitrile solvent molecule was refined as a rigid group. CCDC 1910805-1910812 contains the supplementary crystallographic data for this paper. These data can be obtained free of charge from The Cambridge Crystallographic Data Centre via www.ccdc.cam.ac.uk/structures.

2.2 | General procedure for the synthesis of homonuclear complexes

Homochiral complexes **1**-Λ-(S,S,S,S)-M^{2+}/**1**-Δ-(R,R,R,R)-M^{2+} and **2**-Λ-(S,S,S,S)-M^{2+}/**2**-Δ-(R,R,R,R)-M^{2+} M^{2+} = Zn^{2+}, Fe^{2+}, Co^{2+} have been obtained by template reaction between 2,6-pyridine-dicarboxaldehyde (0.148 mmol) and corresponding chiral amines R-(+)-1- or S-(−)-1-phenylethylamine and R-(+)-1- or S-(−)-1-naphthyl-ethylamine in the presence of stoichiometric amounts of Zn $(CF_3SO_3)_2$, Fe $(BF_4)_2{\cdot}6H_2O$, Co $(BF_4)_2{\cdot}6H_2O$, in acetonitrile, in the molar ratio of aldehyde:amine:metal salt = 1:2:0.5. The reactions were performed typically on a 10-mg scale of ligand per millilitre solvent. The reactants were dissolved in CD_3CN (1 mL) and stirred overnight at 60 °C. These solutions were monitored by ^{1}H-NMR and ESI-mass spectrometries. Layering the solutions of complexes in acetonitrile with isopropyl ether at room temperature resulted in a unique set of single crystals suitable for X-ray single-crystal experiments.

Complex 1-Δ-(R,R,R,R)-Zn^{2+}. Yellow crystals. ^{1}H-RMN (400 MHz, CD_3CN-d_3, δ) 8.22 (s, 4H; CH═N), 7.82-7.80 (d, J = 8 Hz, 4H; H^b), 7.70-7.64 (m, J = 7.2 Hz, J = 8 Hz, 10H; H^a-H^i-H^f), 7.62-7.60 (t, J = 8 Hz, 4H; H^h), 7.56-7.52 (td, J = 8 Hz, 4H; H^g), 7.27-7.25 (d, J = 7.6 Hz, 4H; H^e), 7.07-7.03 (t, J = 7.6 Hz, 4H; H^d), 6.54-6.52 (d, J = 6.4 Hz, J = 7.2 Hz, 4H; H^c), 4.76-4.72 (q, J = 6.8 Hz, 4H; —NCH—), 1.04-1.03 (d, J = 6.4 Hz, 12H; CH_3). UV-vis (acetonitrile 7.425·10^{-5} M): λmax = 282 nm, 220 nm; MS (ESI, *m/z*): 473.36 (100) [Zn(**1**-Δ-(R,R,R,R))$_2$]$^{2+}$, 1095.72 [Zn(**1**-Δ-(R,R,R,R))$_2$](CF_3SO_3)$^+$.

Complex 1-Λ-(S,S,S,S)-Zn^{2+}. Yellow crystals. ^{1}H-RMN (400 MHz, CD_3CN-d_3, δ) 8.22 (s, 4H; CH═N), 7.82-7.80 (d, J = 8 Hz, 4H; H^b), 7.70-7.64 (m, J = 7.2 Hz, J = 8 Hz 10H, H^a-H^i-H^f), 7.62-7.60 (t, J = 8 Hz, 4H; H^h), 7.56-7.52 (td, J = 8 Hz, 4H; H^g), 7.27-7.25 (d, J = 7.6 Hz, 4H, H^e), 7.07-7.03 (t, J = 7.6 Hz, 4H, H^d), 6.54-6.52 (d, J = 6.4 Hz, J = 7.2 Hz, 4H; H^c), 4.77-4.72 (q, J = 6.8 Hz, 4H; —NCH—), 1.04-1.03 (d, J = 6.4 Hz 12H, CH_3). UV-vis (acetonitrile 7.425·10^{-5} M): λmax = 282 nm, 220 nm; MS (ESI, *m/z*): 473.36 (100) [Zn(**1**-Λ-(S,S,S,S))$_2$]$^{2+}$, 1095.78 [Zn(**1**-Λ-(S,S,S,S))$_2$](CF_3SO_3)$^+$.

Complex 1-Δ-(R,R,R,R)-Fe^{2+}. Violet crystals. UV-vis (acetonitrile 7.425·10^{-5} M): λ_{max} = 281 nm (35.57 cm^{-1}, MLCT d-π*), 484 nm (20.67 cm^{-1}), 608 nm (16.45 cm^{-1}), 705 nm (14.2 cm^{-1}). MS (ESI, *m/z*):

TABLE 1 Crystallographic information on data collection and structure refinement

	1-Δ-(R,R,R,R)-Co^{2+}	**1-Λ-(S,S,S,S) Co^{2+}**	**1-Δ-(R,R,R,R)-Fe^{2+}**	**1-Λ-(S,S,S,S) Fe^{2+}**	**1-Δ-(R,R,R,R)-Zn^{2+}**	**1-Λ-(S,S,S,S) Zn^{2+}**	**2-Δ-(R,R,R,R)-Co^{2+}**	**2-Λ-(S,S,S,S) Fe^{2+}**
Formula	$C_{62}H_{54}B_2CoF_8N_6$	$C_{62}H_{54}B_2CoF_8N_6$	$C_{66}H_{60}B_2F_8FeN_8$	$C_{66}H_{60}B_2F_8FeN_8$	$C_{64}H_{54}F_6N_6O_6S_2Zn$	$C_{64}H_{54}F_6N_6O_6S_2Zn$	$C_{48}H_{49}B_2CoF_8N_7$	$C_{50}H_{52}B_2F_8FeN_8$
Moiety	$C_{62}H_{54}CoN_6$,2(BF_4)	$C_{62}H_{54}CoN_6$,2(BF_4)	$C_{62}H_{54}FeN_6$,2(BF_4),2(C_2H_3N)	$C_{62}H_{54}FeN_6$,2(BF_4),2(C_2H_3N)	$C_{62}H_{54}N_6Zn$,2(CF_3O_3S)	$C_{62}H_{54}N_6Zn$,2(CF_3O_3S)	$C_{46}H_{46}CoN_6$,2(BF_4), C_2H_3N	$C_{46}H_{46}FeN_6$,2(BF_4),2(C_2H_3N)
T, K	175	175	175	175	175	175	175	175
Space group	$P6_522$	$P6_122$	$P2_12_12_1$	$P2_12_12_1$	$P22_12_1$	$P22_12_1$	$P2_12_12_1$	$P2_12_12_1$
Crystal system	Hexagonal	Hexagonal	Orthorhombic	Orthorhombic	Orthorhombic	Orthorhombic	Orthorhombic	Orthorhombic
a, Å	12.8190(14)	12.8233(3)	12.68634(16)	12.6784(2)	13.3143(2)	13.3163(2)	11.1126[8]	12.7169(5)
b, Å	12.8190(14)	12.8233(3)	20.5481(3)	20.5187(4)	19.8115(4)	19.8111(4)	12.9994(9)	17.9704(8)
c, Å	59.951(3)	59.9965(15)	21.7836(3)	21.7822(4)	21.1578[5]	21.1606[6]	31.6636(18)	20.5289(10)
α, °	90	90	90	90	90	90	90	90
β, °	90	90	90	90	90	90	90	90
γ, °	120	120	90	90	90	90	90	90
V, $Å^3$	8531.7(5)	8543.9(2)	5678.55(8)	5666.52(11)	5580.92(13)	5582.39(16)	4574.0(3)	4691.4(2)
Z	6	6	4	4	4	4	4	4
ρ, gcm^{-3}	1.303	1.301	1.397	1.400	1.484	1.483	1.389	1.408
M_r, $gmol^{-1}$	1115.66	1115.66	1194.69	1194.69	1246.64	1246.64	956.49	994.47
μ, mm^{-1}	0.373	0.372	0.343	0.344	0.596	0.596	0.451	0.399
R_{int}	0.071	0.094	0.043	0.080	0.103	0.046	0.139	0.166
Θ_{max}, °	33.593	26.371	35.628	32.562	33.606	32.394	26.497	26.372
Resolution, Å	0.68	0.80	0.64	0.66	0.80	0.66	0.80	0.83
N_{tot} (measured)	68 681	44 040	127 786	110 475	46 088	108 276	69 896	71 765
N_{ref} (unique)	21 031	5791	21 371	18 685	19 522	18 278	9440	9602
N_{ref} ($I > 2\sigma(I)$)	6102	4848	17 959	13 252	8854	14 538	6334	5953
N_{ref} (least-squares)	6102	4848	17 959	13 252	8854	14 538	6334	5953
N_{par}	409	409	767	767	767	767	578	623
$<\sigma(I)/I>$	0.1005	0.1344	0.0588	0.1162	0.1845	0.0763	0.1888	0.2220
R_1 ($I > 2\sigma(I)$)	0.0733	0.0897	0.0634	0.0672	0.0742	0.0433	0.0671	0.0858
wR_2 ($I > 2\sigma(I)$)	0.0580	0.0752	0.0678	0.0525	0.0497	0.0431	0.0475	0.0800
R_1 (all)	0.1940	0.1058	0.0774	0.1065	0.1779	0.0639	0.1097	0.1412
wR_2 (all)	0.0734	0.0825	0.0802	0.0550	0.0959	0.0443	0.0663	0.1202
GOF	1.0436	1.0510	1.0756	1.1828	1.0631	1.0657	1.1902	1.1287
$\Delta\rho$ ($eÅ^{-3}$)	−0.88/1.38	−0.83/0.72	−1.11/2.26	−0.96/1.48	−0.88/1.18	−0.57/0.56	−0.54/0.95	−0.51/0.69
Crystal size (mm^3)	0.09 × 0.15 × 0.31	0.07 × 0.24 × 0.24	0.08 × 0.23 × 0.35	0.05 × 0.15 × 0.30	0.08 × 0.12 × 0.23	0.15 × 0.20 × 0.23	0.12 × 0.15 × 0.22	0.05 × 0.12 × 0.21
Flack parameter	0.04(3)	0.11(3)	0.01(1)	0.02(2)	0.02(1)	−0.007(6)	0.00(1)	0.05(4)
Hooft parameter	0.03(2)	0.01(1)	−0.002(4)	−0.008(6)	0.008(6)	−0.0125(1)	−0.01(1)	0.009(9)
Chiral centres	Δ-RRRR	Λ-SSSS	Δ-RRRR	Λ-SSSS	Δ-RRRR	Λ-SSSS	Δ-RRRR	Λ-SSSS

469.33 (100) [Fe(**1**-Δ-(R,R,R,R))$_2$]$^{2+}$, 1025.75 [Fe(**1**-Δ-(R,R,R,R))$_2$](BF$_4$)$^+$.

Complex 1-Λ-(S,S,S,S)-Fe^{2+}. Violet crystals. UV-vis (acetonitrile 7.425·10^{-5} M): λ_{max} = 281 nm (35.57 cm^{-1}, MLCT d-π*), 484 nm (20.67 cm^{-1}), 608 nm (16.45 cm^{-1}). MS (ESI, *m/z*): 469.46 (100) [Fe(**1**-Λ-(S,S,S,S))$_2$]$^{2+}$, 1025.88 [Fe(**1**-Λ-(S,S,S,S))$_2$](BF$_4$)$^+$.

Complex 1-Δ-(R,R,R,R)-Co^{2+}. Brown crystals. UV-vis (acetonitrile 7.425·10^{-5} M): λ_{max} = 281 nm (35.57 cm^{-1}, MLCT d-π*). MS (ESI, *m/z*): 470.88 (100) [Co(**1**-Δ-(R,R,R,R))$_2$]$^{2+}$, 1028.78 [Co(**1**-Δ-(R,R,R,R))$_2$](BF$_4$)$^+$.

Complex 1-Λ-(S,S,S,S)-Co^{2+}. Brown crystals. UV-vis (acetonitrile 7.425·10^{-5} M): λ_{max} = 281 nm (35.57 cm^{-1}, MLCT d-π*). MS (ESI, *m/z*): 470.88 (100) [Co(**1**-Λ-(S,S,S,S))$_2$]$^{2+}$, 1028.78 [Co(**1**-Λ-(S,S,S,S))$_2$](BF$_4$)$^+$.

Complex 2-Δ-(R,R,R,R)-Zn^{2+}. Yellow crystals. ^{1}H-RMN (400 MHz, CD$_3$CN-*d*$_3$, δ) 8.56-8.52 (t, *J* = 7.6 Hz, *J* = 8 Hz, 2H; H^a), 8.30 (s, 4H; CH═N), 8.05-8.03 (d, *J* = 8 Hz, 4H; H^b), 7.20-7.16 (t, *J* = 7.2 Hz, *J* = 7.6 Hz, 4H; H^e), 7.06-7.02 (t, *J* = 8 Hz, J = 7.6 Hz, 8H; H^c), 6.59-6.57 (d, *J* = 7.2 Hz, 8H, H^d), 4.37-4.32 (q, *J* = 6.8 Hz, 4H; NCH—), 1.14-1.13 (d, *J* = 6.8 Hz, 12H; CH$_3$). UV-vis (acetonitrile 7.425·10^{-5} M): λ_{max} = 317 nm, 210 nm; MS (ESI, *m/z*): 373.24 (100) [Zn(**2**-Δ-(R,R,R,R))$_2$]$^{2+}$, 895.55 [Zn(**2**-Δ-(R,R,R,R))$_2$](CF$_3$SO$_3$)$^+$.

Complex 2-Λ-(S,S,S,S)-Zn^{2+}. Yellow crystals. ^{1}H-RMN (400 MHz, CD$_3$CN-*d*$_3$, δ) 8.56-8.52 (t, *J* = 7.6 Hz, *J* = 8 Hz, 2H; H^a), 8.30 (s, 4H; CH═N), 8.05-8.03 (d, *J* = 8 Hz, 4H; H^b), 7.20-7.16 (t, *J* = 7.2 Hz, *J* = 7.6 Hz, 4H; H^e), 7.06-7.02 (t, *J* = 8 Hz, J = 7.6 Hz, 8H; H^c), 6.59-6.57 (d, *J* = 7.2 Hz, 8H, H^d), 4.37-4.32 (q, *J* = 6.8 Hz, 4H; NCH—), 1.14-1.13 (d, *J* = 6.8 Hz, 12H; CH$_3$). UV-vis (acetonitrile 7.425·10^{-5} M): λ_{max} = 318 nm, 210 nm; MS (ESI, *m/z*): 373.24 (100) [Zn(**2**-Λ-(S,S,S,S))$_2$]$^{2+}$, 895.69 [Zn(**2**-Λ-(S,S,S,S))$_2$](CF$_3$SO$_3$)$^+$.

Complex 2-Δ-(R,R,R,R)-Fe^{2+}. Violet crystals. UV-vis (acetonitrile 7.425·10^{-5} M): λ_{max} = 325 nm (30.76 cm^{-1}, MLCT d-π*), 480 nm (20.83 cm^{-1}), 603 nm (16.58 cm^{-1}), 709 nm (14.09 cm^{-1}). MS (ESI, *m/z*): 369.27 (100) [Fe(**2**-Δ-(R,R,R,R))$_2$]$^{2+}$, 825.67 [Fe(**2**-Δ-(R,R,R,R))$_2$](BF$_4$)$^+$.

Complex 2-Λ-(S,S,S,S)-Fe^{2+}. Violet crystals. UV-vis (acetonitrile 7.425·10^{-5} M): λ_{max} = 325 nm (30.76 cm^{-1}, MLCT d-π*), 480 nm (20.83 cm^{-1}), 603 nm (16.58 cm^{-1}), 709 nm (14.09 cm^{-1}). MS (ESI, *m/z*): 369.27 (100) [Fe(**2**-Λ-(S,S,S,S))$_2$]$^{2+}$, 825.67 [Fe(**2**-Λ-(S,S,S,S))$_2$](BF$_4$)$^+$.

Complex 2-Δ-(R,R,R,R)-Co^{2+}. Brown crystals. UV-vis (acetonitrile 7.425·10^{-5} M): λ_{max} = 300 nm (33.32 cm^{-1}, MLCT d-π*). MS (ESI, *m/z*): 370.76 (100) [Co(**2**-Δ-(R,R,R,R))$_2$]$^{2+}$, 828.46 [Co(**2**-Δ-(R,R,R,R))$_2$](BF$_4$)$^+$.

Complex 2-Λ-(S,S,S,S)-Co^{2+}. Brown crystals. UV-vis (acetonitrile 7.425·10^{-5} M): λ_{max} = 302 nm (33.06 cm^{-1}, MLCT d-π*). MS (ESI, *m/z*): 370.76 (100) [Co(**2**-Λ-(S,S,S,S))$_2$]$^{2+}$, 828.77 [Co(**2**-Λ-(S,S,S,S))$_2$](BF$_4$)$^+$.

3 | RESULTS AND DISCUSSION

Mononuclear complexes **1**-Λ-(S,S,S,S)-M^{2+}/**1**-Δ-(R,R,R,R)-M^{2+} and **2**-Λ-(S,S,S,S)-M^{2+}/**2**-Δ-(R,R,R,R)-M^{2+} were obtained *via template* reactions, in the concentration range of 10 mg ligand per 1 mL acetonitrile, from 2,6-pyridinedicarboxaldehyde (1 eq), R-(+)-1-/S-(−)-1-phenylethylamine, and R-(+)-1-/S-(−)-1-naphthyl ethylamine (2 eq) and the corresponding metal ions, Zn^{2+}, Fe^{2+}, Co^{2+} (0.5 eq). The Zn^{2+}, Fe^{2+}, Co^{2+} metal ions used to obtain complexes with in situ generated bis (*arylethyl*imine)pyridine ligands **1** and **2** are ions that prefer octahedral coordination geometry and determine the orthogonal orientation of the ligands similar to that found in the mononuclear metal complexes with the terpyridine ligands. The octahedral complexes of the Zn^{2+}, Fe^{2+}, and Co^{2+} ions are labile and suffer rapid equilibria in solution, and their stability can be correlated with their electronic configuration. On the other hand, the Schiff bases, bis (*aryl*imine)pyridine ligands **1** and **2**, are strong field generators, π-acceptors, with low-energy antibonding orbitals (LUMO, π*), and they form complexes with metal ions stabilized by charge transfer interactions metal(d)-to-ligand(π*) (MLCT).

3.1 | NMR spectroscopy

Only Zn^{2+} ions, d^{10} configuration, form diamagnetic complexes that can be characterized by ^{1}H-NMR spectroscopy. The ^{1}H-NMR spectra of the **1**-Λ-(S,S,S,S)-Zn^{2+}/**1**-Δ-(R,R,R,R)-Zn^{2+} and **2**-Λ-(S,S,S,S)-Zn^{2+}/**2**-Δ-(R,R,R,R)-Zn^{2+} homonuclear complexes (Figures S1 and S2) consist of a series of well-defined peaks characteristic to the 1:2 symmetric metal-ligand complex. In these spectra, the H^a pyridine protons signals of the ligand appear shifted to the weaker magnetic field than the signals corresponding to these protons in similar free bis (*aryl*imine) pyridine ligands.[51-57] Tridentate metal ion coordination determine the ligands to adopt during the *template* synthesis a *cisoid* conformation, corresponding to a terpyridine (terpy) type coordination site. The conversion of the *all-transoid* conformer into the energetically disfavoured *all-cisoid* one upon metal complexation occurs at the cost of conformational energy, which is overcompensated by the interaction energy resulting from metal ion binding.[51-57]

3.2 | ESI-MS spectrometry

Electrospray ionization (ESI) conditions (T = 80 °C, extraction cone voltage V_c = 10 V, 100% acetonitrile) were set to avoid the fragmentation (dissociation) of the complexes. ESI-mass spectra of complexes in acetonitrile solutions (10^{-4} M) showed the formation of double-charged complex ions of $[M(\mathbf{1}\text{-}\Delta\text{-}(R,R,R,R))_2]^{2+}$/$[M(\mathbf{1}\text{-}\Lambda\text{-}(S,S,S,S))_2]^{2+}$ and $[M(\mathbf{2}\text{-}\Delta\text{-}(R,R,R,R))_2]^{2+}$/$[M(\mathbf{2}\text{-}\Lambda\text{-}(S,S,S,S))_2]^{2+}$ at *MW/2* for all metal ions (Zn^{2+}, Fe^{2+}, and Co^{2+}). The primary coordination sphere for metal ions (CN = 6, $[MN_6]$) remains intact in the solution; no substitution reactions with solvent molecules or anions present in the solution occur.

3.3 | Electronic spectra

The information provided by the mass spectra, that in solution are present only the $[M(\mathbf{1}\text{-}\Delta\text{-}(R,R,R,R))_2]^{2+}$/$[M(\mathbf{1}\text{-}\Lambda\text{-}(S,S,S,S))_2]^{2+}$ and $[M(\mathbf{2}\text{-}\Delta\text{-}(R,R,R,R))_2]^{2+}$/$[M(\mathbf{2}\text{-}\Lambda\text{-}(S,S,S,S))_2]^{2+}$ complexes, namely, the primary coordination sphere of the metal ion is formed exclusively from the nitrogen atoms of the tridentate ligands, allow assignment of the *d-d* transitions for Fe^{2+} and Co^{2+} complexes (Table 2) from electronic UV-Vis spectra in solution. In octahedral coordination geometry, Fe^{2+} metal ions can present two spin states, depending on the strength of the ligand field, with the following fundamental spectral terms: $^1A_{1g}$ (LS) and $^5T_{2g}$ (HS). For the Co^{2+} metal ion, in octahedral symmetry, the fundamental spectral terms are ^2E (LS) and $^4T_{1g}$ (HS).

The UV-Vis spectra of the **1**-Λ-(S,S,S,S)-Fe^{2+}/**1**-Δ-(R,R,R,R)-Fe^{2+} and **2**-Λ-(S,S,S,S)-Fe^{2+}/**2**-Δ-(R,R,R,R)-Fe^{2+} complexes have absorption maxima specific to the low-spin (LS) distorted octahedral geometries for Fe^{2+} ions. In these spectra, $^1A_{1g} \rightarrow {}^1T_{1g}$ and $^1A_{1g} \rightarrow {}^1T_{2g}$ are assigned to the spin-allowed transitions. The weaker bands at 608 nm and 705 nm were assigned to spin-forbidden transitions to triplet terms ($^3T_{1g}$, $^3T^{2g}$). The bis (*arylethyl*imino)pyridine ligands, **1** and **2**, are strong field generators, π acceptors, with antibonding orbitals (LUMO, π*) low in energy, and they form complexes stabilized by metal-to-ligand interactions (MLCT). MLCT bands for octahedral Fe^{2+} ion, d^6 occur in the low-energy domain approximately 30 kK and are very characteristic to the red-violet LS complexes of Fe^{2+} with ligands similar to bis (*arylethyl*imino)pyridines: bypiridine (bpy) and phenanthroline (1,10-phen), $[Fe\ (bpy)_3]^{2+}$, $Fe(1,10\text{-}phen)_3]^{2+}$.

Similar shifting of these MLCT bands and the brown colour in **1**-Λ-(S,S,S,S)-Co^{2+}/**1**-Δ-(R,R,R,R)-Co^{2+} and **2**-Λ-(S,S,S,S)-Co^{2+}/**2**-Δ-(R,R,R,R)-Co^{2+} complexes are observed and are due to the strong field behaviour of bis (*arylethyl*imino)pyridine ligands, **1** and **2**, in a similar manner to other Co^{2+}-complexes with related ligands: $[Co\ (bpy)_3]^{2+}$ and $[Co(1,10\text{-}phen)_3]^{2+}$. For all Co^{2+} complexes, the spin-allowed transitions are obscured by MLCT bands.

3.4 | CD spectra

The CD spectra measured in acetonitrile confirm the optical activity and enantiomeric nature of **1**-Λ-(S,S,S,S)-M^{2+}/**1**-Δ-(R,R,R,R)-M^{2+} and **2**-Λ-(S,S,S,S)-M^{2+}/**2**-Δ-(R,R,R,R)-M^{2+} chiral complexes (Figure 1):

- In acetonitrile solution, the complexes retain their chirality as the enantiomeric pairs present the same absorption maxima with opposite signs. Their spectra show negative or positive Cotton effects depending on the sense of chirality.
- The absorption bands in the spectra of the **2**-Λ-(S,S,S,S)-M^{2+}/**2**-Δ-(R,R,R,R)-M^{2+} complexes are weaker in intensity compared with those in the spectra of

TABLE 2 *d-d* spin-allowed transitions and MLCT bands for **1**-Λ-(S,S,S,S)-M^{2+}/**1**-Δ-(R,R,R,R)-M^{2+} and **2**-Λ-(S,S,S,S)-M^{2+}/**2**-Δ-(R,R,R,R)-M^{2+}, M = Co^{2+}, Fe^{2+}

Complex	**1-Δ-(R,R,R,R)-Fe^{2+}**	**1-Λ-(S,S,S,S)-Fe^{2+}**	**2-Δ-(R,R,R,R)-Fe^{2+}**	**2-Λ-(S,S,S,S)-Fe^{2+}**	**1-Δ-(R,R,R,R)-Co^{2+}/1-Λ-(S,S,S,S)-Co^{2+}**	**2-Δ-(R,R,R,R)-Co^{2+}**	**2-Λ-(S,S,S,S)-Co^{2+}**
Transitions, kK	35.57 (281 nm) $^1A_{1g} \rightarrow {}^1T_{2g}$ (MLCT d-π*) 20.67 (484 nm) $^1A_{1g} \rightarrow {}^1T_{1g}$ 16.45 (608 nm) $^1A_{1g} \rightarrow {}^3T_{1g}$ 14.2 (705 nm) $^1A_{1g} \rightarrow {}^3T_{2g}$	35.57 (281 nm) $^1A_{1g} \rightarrow {}^1T_{2g}$ (MLCT d-π*) 20.67 (484 nm) $^1A_{1g} \rightarrow {}^1T_{1g}$ 16.45 (608 nm) $^1A_{1g} \rightarrow {}^3T_{1g}$	30.76 (325 nm) $^1A_{1g} \rightarrow {}^1T_{2g}$ (MLCT d-π*) 20.83 (480 nm) $^1A_{1g} \rightarrow {}^1T_{1g}$ 16.58 (603 nm) $^1A_{1g} \rightarrow {}^3T_{1g}$ 14.09 (710 nm) $^1A_{1g} \rightarrow {}^3T_{2g}$	30.76 (325 nm) $^1A_{1g} \rightarrow {}^1T_{2g}$ (MLCT d-π*) 20.83 (480 nm) $^1A_{1g} \rightarrow {}^1T_{1g}$ 16.58 (603 nm) $^1A_{1g} \rightarrow {}^3T_{1g}$ 14.2 (705 nm) $^1A_{1g} \rightarrow {}^3T_{2g}$	35.57 (281 nm) MLCT d-π*	33.32 (300 nm) MLCT d-π*	33.06 (303 nm) MLCT d-π*

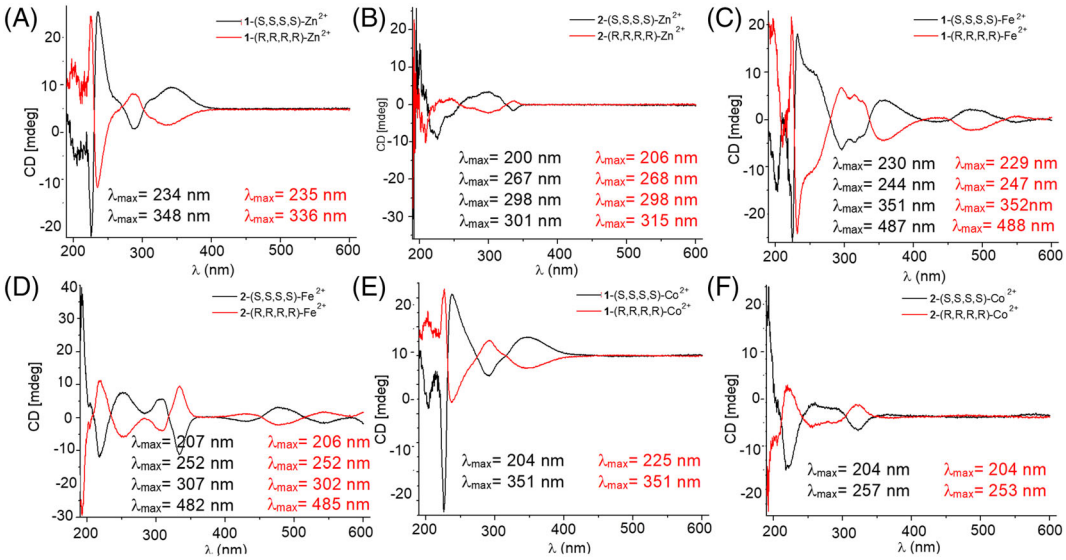

FIGURE 1 The CD spectra measured in acetonitrile solutions of (A) **1**-Λ-(S,S,S,S)-Zn^{2+}/**1**-Δ-(R,R,R,R)-Zn^{2+}; (B) **2**-Λ-(S,S,S,S)-Zn^{2+}/**2**-Δ-(R,R,R,R)-Zn^{2+}; (C) **1**-Λ-(S,S,S,S)-Fe^{2+}/**1**-Δ-(R,R,R,R)-Fe^{2+}; (D) **2**-Λ-(S,S,S,S)-Fe^{2+}/**2**-Δ-(R,R,R,R)-Fe^{2+}; (E) **1**-Λ-(S,S,S,S)-Co^{2+}/**1**-Δ-(R,R,R,R)-Co^{2+}; and (F) **2**-Λ-(S,S,S,S)-Co^{2+}/**2**-Δ-(R,R,R,R)-Co^{2+} complexes

1-Λ-(S,S,S,S)-M^{2+}/**1**-Δ-(R,R,R,R)-M^{2+}. This fact may be correlated with the better π-acceptor character of the ligand **1** and, consequently, with the ability to exert a stronger field in its complexes. In a series of ligands with aromatic constituents, the antibonding orbital (LUMO, π*) is at lower energy values as the conjugate system is more extended; therefore, the LUMO orbitals are energetically closer to the metal orbital t_{2g}, and the overlapping π metal-ligand is strong. The result of this stronger interaction with the π-acceptor ligand is an increase in transition energy.

- The absorption bands with maxima situated around 485 nm are present both in DC and UV-vis spectra of Fe^{2+} complexes (Figure 1C,D). These absorption bands were attributed to the spin-allowed transition $^1A_{1g} \rightarrow {}^1T_{1g}$ for Fe^{2+}, d^6, LS.
- For the Zn^{2+} complexes (Figure 1A,B), in the absence of crystal field stabilisation energy (CFSE) (d^{10}), the absorption bands are attributed to the allowed electronic transitions ^1L_a and ^1B_b from the chromophore moieties of the chiral ligands **1** and **2**: ^1L_a = 200 nm and 206 nm, ^1B_b = 267-268 nm for phenyl chromophore, ^1L_a = 234 to 235 nm, ^1B_b = 348 and 336 nm for naphthyl chromophore.[57] Compared with the CD spectra of the constituent chromophores of the ligands, the chiral amines R-(+)-1-/S-(−) -1-phenylethylamine and R-(+)-1-/S-(−)-1-naphthylethylamine), these maxima are red-shifted (^1B_b = 269 nm, 261 nm-**phenyl**, ^1B_b = 336 nm, 282 nm-**naphthyl**), probably because of the electronic interactions (charge transfer or π-π stacking) chromophore-pyridine.[70,71] The same behaviour also occurs in the CD spectra of Fe^{2+} (Figure 1C,D) and Co^{2+} (Figure 1E,F) complexes.

3.5 | X-ray single crystal diffraction structures

The crystal structures of the complexes **1**-Λ-(S,S,S,S)-M^{2+}/**1**-Δ-(R,R,R,R)-M^{2+} M^{2+} = Co^{2+}, Fe^{2+}, Zn^{2+}, **2**-Λ-(S,S,S,S)-Fe^{2+} and **2**-Δ-(R,R,R,R)-Co^{2+} were determined from crystals obtained from the acetonitrile/*i*-propylether solutions at room temperature. Labelled asymmetric units and selected bond lengths and angles are described in Tables S1 to S4. The molecular and the crystal packing structures are presented in Figures 2–5.

1-Λ-(S,S,S,S)-Zn^{2+} and **1**-Δ-(R,R,R,R)-Zn^{2+} complexes belong to the orthorhombic non-centrosymmetric space group $P22_12_1$ (#18), and the crystallographic data are listed in Table S1. The asymmetric unit consists in both cases of [**1**-Λ-(S,S,S,S)-Zn]$^{2+}$ or [**1**-Δ-(R,R,R,R)-Zn]$^{2+}$ cations and two $CF_3SO_3^-$ anions. The Zn^{2+}-$N_{Pyridine}$ and Zn^{2+}-N_{imine} distances vary between 2.002[4] to 2.013[4] Å and 2.2587[17] to 2.4055[17] Å, respectively.

1-Λ-(S,S,S,S)-Fe^{2+} and **1**-Δ-(R,R,R,R)-Fe^{2+} complexes crystallize in the orthorhombic non-centrosymmetric space group $P2_12_12_1$ (#19) (Table S2). The asymmetric unit consists in both cases of [**1**-Λ-(S,S,S,S)-Fe]$^{2+}$ or [**1**-Δ-(R,R,R,R)-Fe]$^{2+}$ cations, two BF_4^- anions, and two acetonitrile molecules. The geometric parameters imply that **1**-Λ-(S,S,S,S)-Fe^{2+} and **1**-Δ-(R,R,R,R)-Fe^{2+} complexes

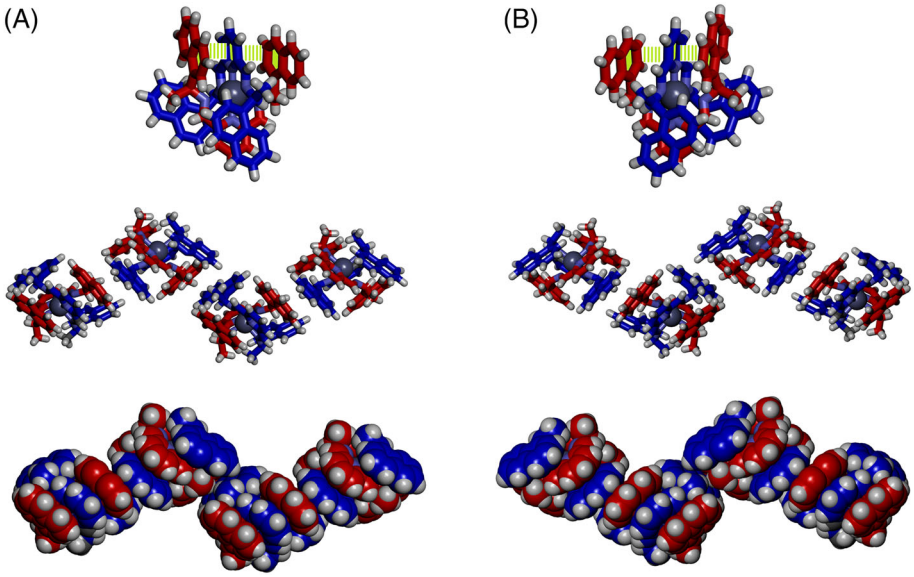

FIGURE 2 Homochiral duplexes (top) and side view in stick (middle) and CPK (bottom) representation of the crystal packing of (A) **1**-Λ-(S,S,S,S)-Zn^{2+} and (B) **1**-Δ-(R,R,R,R)Zn^{2+} complexes. Green lines represent π-π interactions

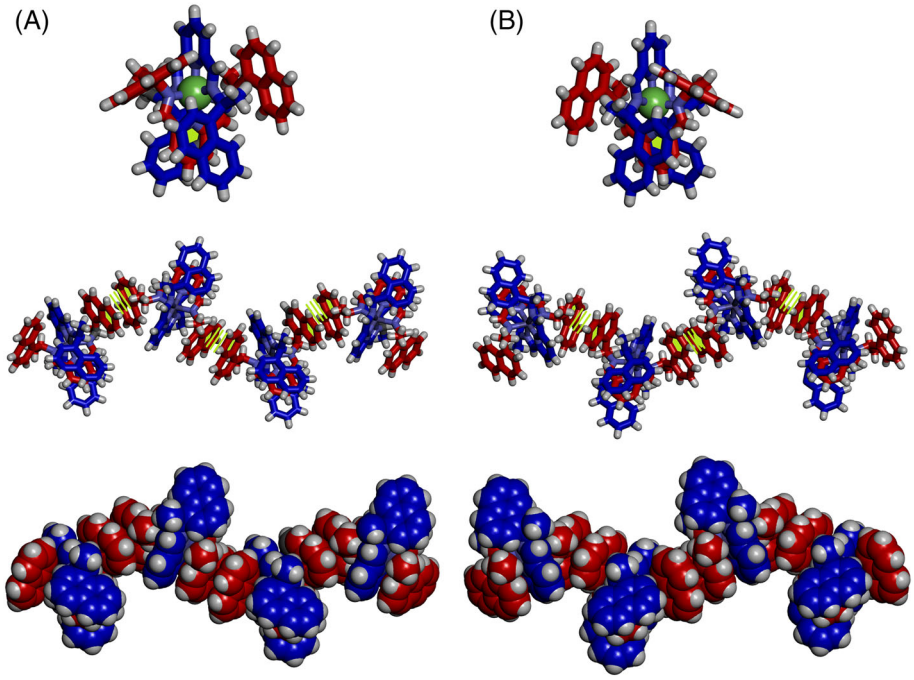

FIGURE 3 Homochiral duplexes (top) and side view in stick (middle) and CPK (bottom) representation of the crystal packing of (A) **1**-Λ-(S,S,S,S)-Fe^{2+} and (B) **1**-Δ-(R,R,R,R)-Fe^{2+} complexes. Green lines represent π-π interactions

are low spin at 175 K and the Fe-N distances are of typical values for LS complexes of Fe^{2+} with pyridine-type ligands. The average Fe^{2+}-$N_{Pyridine}$ and Fe^{2+}-N_{imine} distances are 1.8519[17] to 1.880[2] Å and 1.9457[17] to 2.1073[18] Å, respectively.

1-Λ-(S,S,S,S)-Co^{2+} and **1**-Δ-(R,R,R,R)-Co^{2+} crystals belong to the enantiomorphic space group pair $P6_122$/$P6_522$. The asymmetric unit consists in both cases of [**1**-Λ-(S,S,S,S)-Co]$^{2+}$ and [**1**-Δ-(R,R,R,R)-Co]$^{2+}$ cations and two BF_4^- anions (Table S3). The Co—N distances, Co^{2+}-$N_{Pyridine}$ = 1.848[3] to 1.925[5] Å and Co^{2+}-N_{imine} = 2.017[3] to 2.318[4] Å, indicate that **1**-Λ-(S,S,S,S)-Co^{2+} and **1**-Δ-(R,R,R,R)-Co^{2+} are, as expected, low-spin complexes at 175 K.

2-Λ-(S,S,S,S)-Fe^{2+} and **2**-Δ-(R,R,R,R)-Co^{2+} crystallize in the orthorhombic non-centrosymmetric space group $P2_12_12_1$ (#19) (Table S4). Each Fe^{2+}/Co^{2+} ion binds two *bis* (phenylethylimine)pyridine ligands, **2,** and has a

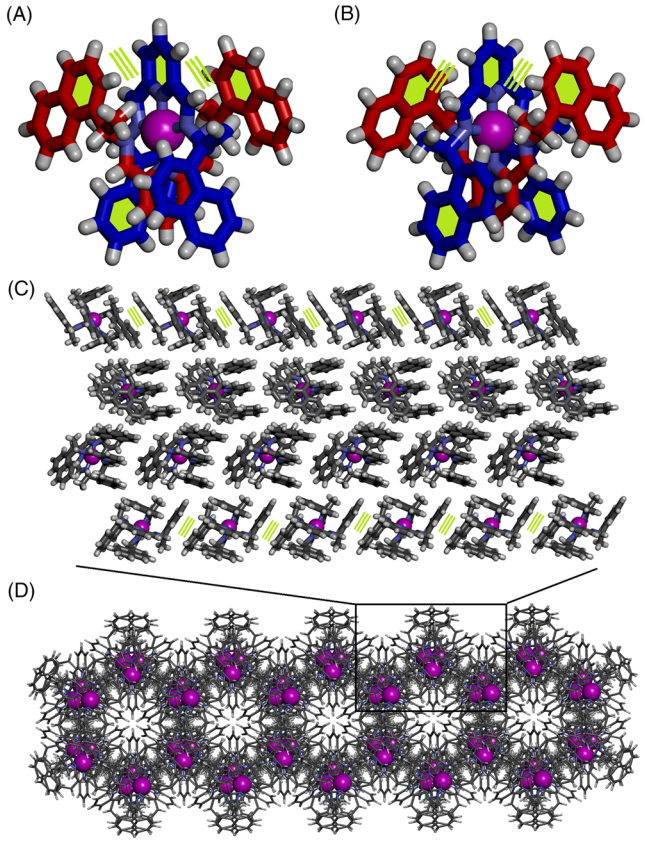

FIGURE 4 Homochiral duplexes (A) **1**-Λ-(S,S,S,S)-Co^{2+} and (B) **1**-Δ-(R,R,R,R)-Co^{2+}; (C) side view and (D) top view in stick representation of the crystal packing of complexes. Green lines represent π-π interactions

pseudo-octahedral coordination geometry, but the complexes did not crystallize similarly: Both complexes are solvates, but **2**-Δ-(R,R,R,R)-Co^{2+} crystallizes with only one acetonitrile solvent molecule, whereas two acetonitrile molecules are present in the structure of **2**-Λ-(S,S,S,S)-Fe^{2+}.

In all duplex structures, the M^{2+} metal ions are fully coordinated by two ligands arranged into orthogonal planes and present an octahedral coordination geometry. Each ligand in the *all-cis* configuration serves as a tridentate ligand and coordinates meridionally to the metal ion with one pyridine and two imine nitrogen atoms. Continuous shape measurements analysis[72,73] showed that all transition metal ions, M^{2+} = Zn^{2+}, Fe^{2+}, Co^{2+}, display distorted octahedral coordination environments (Table S5, Figures S3 and S4), and among these, Fe^{2+} complexes (LS, d^6) are the less distorted from ideal octahedron, whereas Co^{2+} (LS, d^7) with one electron in the antibonding e_g orbitals and Zn^{2+} (d^{10}) present greater degrees of distortion.

For **1**-Λ-(S,S,S,S)-M^{2+}/**1**-Δ-(R,R,R,R)-M^{2+}, whereas the average Fe^{2+}-$N_{Pyridine}$ and Co^{2+}-$N_{Pyridine}$ distances are similar, 1.852/1.848 Å, the average Zn^{2+}-$N_{Pyridine}$ distance is much longer: 2.002 Å. The M^{2+}-N_{imine} distances are progressively increasing as following: Fe^{2+}-N_{imine} < Co^{2+}-N_{imine} < Zn^{2+}-N_{imine} distances of 1.946, 2.017, and 2.258 Å, respectively. These fairly different geometrical parameters and the M^{2+} coordination behaviour (ie, distorted symmetry for Fe^{2+}/Co^{2+} and the lack of CFSE for Zn^{2+}) lead to slight differences in the spatial disposition of lateral naphthyl arms. As an important consequence, the double helix complexes are not isostructural: They crystallize in different space groups ($P22_12_1$, $P2_12_12_1$, and $P6_122$/$P6_522$, respectively). This fact is more evident for the crystals of enantiomeric pairs **1**-Λ-(S,S,S,S)-Fe^{2+}/**1**-Δ-(R,R,R,R)-Fe^{2+} and **1**-Λ-(S,S,S,S)-Co^{2+}/**1**-Δ-(R,R,R,R)-Co^{2+} that are not isostructural, although they have been synthesized under identical conditions: same solvent system (CD_3CN/*i*-propylether) and same counterion (BF_4^-).

The methyl-CH^* chiral spacer in the structure of the ligands is important for holding and stabilizing the duplex formation by the internal π-π stacking. As a general rule, in the crystal, the two ligands are strongly intertwined, stabilizing the duplex superstructures by internal π-π stacking interactions. The relative position

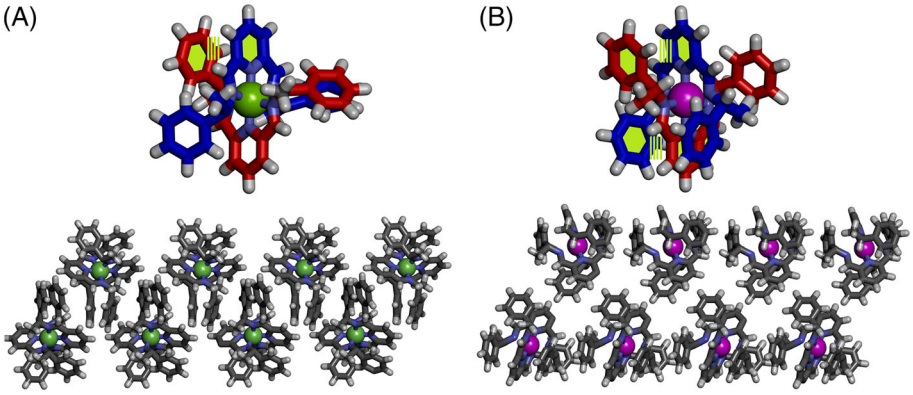

FIGURE 5 Homochiral duplexes (top) and side view of the crystal packing (bottom) of (A) **2**-Λ-(S,S,S,S)-Fe^{2+} and (B) **2**-Δ-(R,R,R,R)-Co^{2+} complexes

of the duplex ligands allows a *partial* (**1**-Λ-(S,S,S,S)-Fe^{2+}, **1**-Δ-(R,R,R,R)Fe^{2+}, **2**-Λ-(S,S,S,S)-Fe^{2+}, and **2**-Δ-(R,R,R,R)-Co^{2+}) or a *total* (**1**-Λ-(S,S,S,S)-Zn^{2+}, **1**-Δ-(R,R,R,R)-Zn^{2+}, **1**-Λ-(S,S,S,S)-Co^{2+}, and **1**-Δ-(R,R,R,R)-Co^{2+}) internal overlap between the naphthyl or phenyl moieties and the central pyridine moiety of a vicinal ligand via π-π stacking aromatic interactions with an average centroid-centroid distances of 3.4-3.7 Å, corresponding to van der Waals contacts: face-to-face π-π, heteroaromatic (py)-aromatic interactions, and CH⋯π (y-interaction) (Figures S5 to S8).[74]

Between peripheral aromatic rings (*naphthyl* for **1**-Λ-(S,S,S,S)-M^{2+}/**1**-Δ-(R,R,R,R)-M^{2+}or *phenyl* for **2**-Λ-(S,S,S,S)-Fe^{2+} and **2**-Δ-(R,R,R,R)-Co^{2+}) intermolecular associations through CH⋯π (T-interaction) with average centroid-edge distances of 3.4-3.7 Å are established (Figures S5 to S8).[74]

In the case of partial internal overlap, the external π-π stacking interactions are occurring between communicating duplex structures. It is resulting in the formation of left-handed **1**-Λ-(S,S,S,S)-Fe^{2+} (Figure 3), **2**-Λ-(S,S,S,S)-Fe^{2+}) (Figure 5) or right-handed **1**-Δ-(R,R,R,R)-Fe^{2+} (Figure 3), and **2**-Δ-(R,R,R,R)-Co^{2+} (Figure 5), single helix superstructures that are present in the crystal structure.

In a different manner, in the crystals of **1**-Λ-(S,S,S,S)-Zn^{2+}, **1**-Δ-(R,R,R,R)-Zn^{2+}, **1**-Λ-(S,S,S,S)-Co^{2+}, and **1**-Δ-(R,R,R,R)Co^{2+} complexes, the communication between duplexes, which are mostly internally stacked, is disrupted; each duplex being closely packed with two neighbouring ones by weak van der Waals contacts while the external π-π stacking aromatic interactions are completely suppressed in the frameworks (Figures 2 and 4).

4 | CONCLUSION

In conclusion, we have demonstrated in this paper that the molecular chirality is transferred to chiral duplex superstructures that can be generated in solution and solid-state single-crystals *via* a combination of metal-ion coordination and weak π-π stacking and van der Waals interactions. Hierarchical supramolecular organization is promoted by the formation of metallosupramolecular duplexes, stabilized by internal π-π stacking. The introduction of a chiral spacer between imine moiety and aryl groups induces a spatial orientation of the lateral aromatic arms that is clearly important for internal holding and stabilization of the duplex formation by π-π stacking. When such internal interactions are dominant, the external π-π stacking communication is completely removed, and non-communicating duplex structures are present in the crystal. Long-range 3D supramolecular structure propagation is favoured when both partial internal overlapping and external π-π stacking are present, leading to the formation of robust single-helical configurations or tubular packed architectures. The use of multiple supramolecular interactions provides a very powerful platform for the transfer of chiral information from molecular to supramolecular level. The internal robustness of the duplexes is mainly responsible for the transmission of the supramolecular homochiral order and is reminiscent with sliding biological processes along homochiral 3D hypersurfaces occurring in the formation of chiral biological relevant species at the nanolevel.[75-77]

ACKNOWLEDGEMENTS

This work was supported by Agence Nationale de la Recherche ANR-15-CE29-0009 DYNAFUN.

ORCID

Mihail Barboiu https://orcid.org/0000-0003-0042-9483

REFERENCES

1. Amouri H, Gruselle M. *Chirality in Transition Metal Chemistry: Molecules, Supramolecular Assemblies and Materials*. New York: John Wiley & Sons; 2008.
2. Zhang X, Yin J, Yoon J. Recent advances in development of chiral fluorescent and colorimetric sensors. *Chem Rev*. 2014;114(9):4918-4959.
3. Dragna JM, Pescitelli G, Tran L, Lynch VM, Anslyn EV, Di Bari L. In situ assembly of octahedral Fe^{2+} complexes for the enantiomeric excess determination of chiral amines using circular dichroism spectroscopy. *J Am Chem Soc*. 2012;134(9):4398-4407.
4. Nieto S, Dragna JM, Anslyn EV. A facile CD protocol for rapid determination of enantiomeric excess and concentration of chiral primary amines. *Chem A Eur J*. 2010;16(1):227-232.
5. Dragna JM, Gade AM, Tran L, Lynch VM, Anslyn EV. Chiral amine enantiomeric excess determination using self-assembled octahedral Fe^{2+}-imine complexes. *Chirality*. 2015;27(4):294-298.
6. Chen X, Lu Z. Recent advances in chiral imino-containing ligands for metal-catalyzed asymmetric transformations. *Org Biomol Chem*. 2017;15(11):2280-2306.
7. Cruchter T, Larionov VA. Asymmetric catalysis with octahedral stereogenic-at-metal complexes featuring chiral ligands. *Coord Chem Rev*. 2018;376:95-113.
8. Crassous J. Chiral transfer in coordination complexes: towards molecular materials. *Chem Soc Rev*. 2009;38(3):830-845.
9. Aritake Y, Nakayama T, Nishizuru H, Akitsu T. Observation of induced CD on CdSe nanoparticles from chiral Schiff base Ni^{2+}, Cu^{2+} Zn^{2+}complexes. *Inorg Chem Comm*. 2011;14(2):423-425.
10. Aritake Y, Takanashi T, Yamazaki A, Akitsu T. Polarized spectroscopy and hybrid materials of chiral Schiff base Ni(2+),

Cu(2+), Zn(2+) complexes with included or separated azo-groups. *Polyhedron*. 2011;30(5):886-894.

11. Akitsu T, Itoh T. Polarized spectroscopy of hybrid materials of chiral Schiff base cobalt(2+), nickel(2+), copper(2+), and zinc(2+) complexes and photochromic azobenzenes in PMMA films. *Polyhedron*. 2010;29(1):477-487.
12. Akitsu T. Photofunctional supramolecular solution systems of chiral Schiff base nickel(2+), copper(2+), and zinc(2+) complexes and photochromic azobenzenes. *Polyhedron*. 2007;26 (12):2527-2535.
13. Onodera T, Akitsu T. Tuning of the optical properties of chiral Schiff base Zn(2+) complexes by substituents. *Polyhedron*. 2013;59:107-114.
14. Albert J, Magali Cadena J, Granell JR, Solans X, Font-Bardia M. Optically active palladacycles containing imines derived from 1-(1-naphthyl)ethylamine: new resolving agents for P-chiral phosphines. *Tetrahedron Asymmetry*. 2000;11(9):1943-1955.
15. Benito M, López C, Solans X, Font-Bardía M. Palladium(2+) compounds with planar chirality. X-ray crystal structures of (+)-(*R*)-[{(η^5-C_5H_4)—CH=N—CH (Me)—$C_{10}H_7$}Fe(η^5-C_5H_5)] and (+)-(R_p,*R*)-[Pd{[(Et—C=C—Et)$_2$(η^5-C_5H_3)—CH=N—CH (Me)—$C_{10}H_7$]Fe(η^5-C_5H_5)}Cl]. *Tetrahedron Asymmetry*. 1998;9 (23):4219-4238.
16. Bao L-Y, Hao S-J, Xi S-F, et al. Chiral supramolecular coordination cages as high-performance inhibitors against amyloid-β aggregation. *Chem Commun*. 2018;54(63):8725-8728.
17. Zhou X-Q, Li Y, Zhang D-Y, et al. Copper complexes based on chiral Schiff-base ligands: DNA/BSA binding ability, DNA cleavage activity, cytotoxicity and mechanism of apoptosis. *Eur J Med Chem*. 2016;114:244-256.
18. Anderson C, Crespo M, Rochon FD. Stereoselective oxidative addition of methyl iodide to chiral cyclometallated Pt^{2+} compounds derived from (*R*)-(+)-1-(1-naphthyl ethylamine). Crystal structure of [PtMe{3-(*R*)-($C_{10}H_7$)CHMeNCHC$_4$H$_2$S}PPh$_3$]. *J Organomet Chem*. 2001;631(1-2):164-174.
19. Khan NH, Pandya N, Prathap KJ, et al. Chiral discrimination asserted by enantiomers of Ni(2+), Cu(2+) and Zn(2+) Schiff base complexes in DNA binding, antioxidant and antibacterial activities. *Spectrochim Acta A Mol Biomol Spectrosc*. 2011;81(1):199-208.
20. Muppidi VK, Zacharias PS, Pal S. Self-assembly of a pseudo-tetrahedral Zn(2+) complex with a chiral reduced Schiff base into a helical superstructure. *Inorg Chem Commun*. 2005;8 (6):543-547.
21. Strong ETJ, Price JT, Jones ND. Modular syntheses of chiral and achiral *C,N*-chelated Pd(2+)-pyridinylidenes. *Dalton Trans*. 2009;38(42):9123-9125.
22. Iglesias AL, Aguirre G, Somanathan R, Parra-Hake M. New chiral Schiff base–Cu(2+) complexes as cyclopropanation catalysts. *Polyhedron*. 2004;23(18):3051-3062.
23. Becerra A, Contreras R, Carmona D, Lahoz FJ, Garcia-Orduna P. Half-sandwich rhodium and iridium complexes containing homochiral imidazolyl-imine ligands: synthesis, characterization and catalytic applications. *Dalton Trans*. 2013;42(32): 11640-11651.
24. Carmona D, Lahoz FJ, Elipe S, et al. Synthesis, characterization, properties, and asymmetric catalytic Diels-Alder reactions of chiral-at-metal imino−iridium(2 + I) complexes. *Organometallics*. 1998;17(14):2986-2995.
25. Anderson C, Crespo M, Morris J, Tanski JM. Reactivity of cyclometallated platinum complexes with chiral ligands. *J Organomet Chem*. 2006;691(26):5635-5641.
26. Constable EC, Zhang G, Housecroft CE, Neuburger M, Zampese JA. π-Stacking and hydrogen bonding direct diastereoselectivity in one-pot syntheses of octahedral iron(2+) complexes. *Chem Commun*. 2010;46(18):3077-3079.
27. Gu Z-G, Na J-J, Bao F-F, et al. Synthesis, characterization, and DNA-binding of enantiomers of iron(2+) Schiff base complexes. *Polyhedron*. 2013;51:186-191.
28. Pescitelli G, Ludeke S, Chamayou A-C, et al. Broad-range spectral analysis for chiral metal coordination compounds: (chiro) optical superspectrum of cobalt(2+) complexes. *Inorg Chem*. 2018;57(21):13397-13408.
29. Daneshmand P, Michalsky I, Aguiar PM, Schaper F. Configurationally flexible zinc complexes as catalysts for *rac*-lactide polymerisation. *Dalton Trans*. 2018;47(45):16279-16291.
30. Li T-Y, Zheng Y-X, Zhou Y-H. Iridium(2 + I) phosphorescent complexes with dual stereogenic centers: single crystal, electronic circular dichroism evidence and circularly polarized luminescence properties. *Dalton Trans*. 2016;45(48): 19234-19237.
31. Han W-K, Qin L-F, Pang C-Y, et al. Polymorphism of a chiral iron(2+) complex: spin-crossover and ferroelectric properties. *Dalton Trans*. 2017;46(25):8004-8008.
32. Jia B, Hao J, Wei X, Tong H, Zhou M, Liu D. Zinc and aluminum complexes of chiral ligands: Synthesis, characterization and application to rac-lactide polymerization. *JOrganometChem*. 2017;831:11-17.
33. Albert J, D'Andrea L, Granell J, Tavera R, Font-Bardia M, Solans X. Synthesis and reactivity towards carbon monoxide of an optically active *endo* five-membered *ortho*-cyclopalladated imine: X-ray molecular structure of *trans*-(μ-Cl)$_2$[Pd(κ^2-*C,N*-(*R*)-C_6H_4-CH=N-CHMe-Ph)]$_2$. *J Organomet Chem*. 2007;692 (14):3070-3080.
34. Fossey JS, Russell ML, Malik KMA, Richards CJ. Synthesis and crystal structures of the first C_2-symmetric bis-aldimine *NCN*–pincer complexes of platinum and palladium. *J Organomet Chem*. 2007;692(22):4843-4848.
35. Howson SE, Allan LEN, Chmel NP, et al. Origins of stereoselectivity in optically pure phenylethanimino-pyridine*tris*-chelates M (NN′)$_3^{n+}$ (M=Mn, Fe, Co, Ni and Zn). *Dalton Trans*. 2011;40(40):10416-10433.
36. Gu Z-G, Pang C-Y, Qiu D, et al. Homochiral iron(2+) complexes based on imidazole Schiff-base ligands: syntheses, structures, and spin-crossover properties. *Inorg Chem Commun*. 2013;35:164-168.
37. Pait M, Shatruk M, Lengyel J, et al. Two types of nitrito support for μ_4-oxido-bridged [Cu$_4$] complexes: synthesis, crystal structures, magnetic properties and DFT analysis. *Dalton Trans*. 2015;44(13):6107-6117.
38. Zhang F-L, Tian L, Qin L-F, et al. Chiral double helical silver complexes: subcomponent self-assembly and self-sorting. *Polyhedron*. 2016;104:9-16.

39. Pastor MF, Whitehorne TJJ, Oguadinma PO, Schaper F. Zinc complexes of chiral ligands obtained from methylbenzylamine. *Inorg Chem Commun*. 2011;14(11):1737-1741.
40. Qin L-F, Pang C-Y, Han W-K, et al. Spin crossover properties of enantiomers, co-enantiomers, racemates, and co-racemates. *Dalton Trans*. 2016;45(17):7340-7348.
41. Li L, Becker JM, Allan LEN, Clarkson GJ, Turner SS, Scott P. Structural and electronic modulation of magnetic properties in a family of chiral iron coordination polymers. *Inorg Chem*. 2011;50(13):5925-5935.
42. Han W-K, Li Z-H, Zhu W, et al. Molecular isomerism induced Fe(2+) spin state difference based on the tautomerization of the 4(5)-methylimidazole group. *Dalton Trans*. 2017;46(13):4218-4224.
43. Min KS, Park AH, Shin JW, Rowthu SR, Kim SK, Ryoo JJ. Synthesis and characterization of enantiopure copper(2+) complexes using chiral bidentate ligands. *Dalton Trans*. 2010;39(37):8741-8747.
44. Mamula O, von Zelewsky A, Bark T, Stoeckli-Evans H, Neels A, Bernardinelli G. Predetermined chirality at metal centers of various coordination geometries: a chiral cleft ligand for tetrahedral (T-4), square-planar (SP-4), trigonal-bipyramidal (TB-5), square-pyramidal (SPY-5), and octahedral (OC-6) complexes. *Chem A Eur J*. 2000;6(19):3575-3585.
45. Knof U, von Zelewsky A. Predetermined chirality at metal centers. *Angew Chem Int Ed Engl*. 1999;38(3):302-322.
46. Liu M, Zhang L, Wang T. Supramolecular chirality in self-assembled systems. *Chem Rev*. 2015;115(15):7304-7397.
47. Crusats J, Veintemillas-Verdaguer S, Ribo JM. Homochirality as a consequence of thermodynamic equilibrium? *Chem A Eur J*. 2006;12(30):7776-7781.
48. Chen L-J, Yang H-B, Shionoya M. Chiral metallosupramolecular architectures. *Chem Soc Rev*. 2017;46(9):2555-2576.
49. Ohkita M, Lehn J-M, Baum G, Fenske D. Helicity coding: programmed molecular self-organization of achiral nonbiological strands into multiturn helical superstructures: synthesis and characterization of alternating pyridine-pyrimidine oligomers. *Chem A Eur J*. 1999;5(12):3471-3481.
50. Kramer R, Lehn J-M, De Cian A, Fischer J. Self-Assembly, Structure, and Spontaneous Resolution of a Trinuclear Triple Helix from an Oligobipyridine Ligand and NiII Ions. *Angew Chem Int Ed Engl*. 1993;32(5):703-706.
51. Dumitru F, Legrand Y-M, van der Lee A, Barboiu M. Constitutional self-sorting of homochiral supramolecular helical single-crystals from achiral components. *Chem Commun*. 2009;19:2667-2669.
52. Barboiu M, Dumitru F, Legrand Y-M, Petit E, van der Lee A. Self-sorting of equilibrating metallosupramolecular DCLs via constitutional crystallization. *Chem Commun*. 2009;16:2192-2194.
53. Dumitru F, Legrand Y-M, Barboiu M, van der Lee A. Weak intermolecular hydrogen and halogen interactions in an isomorphous halogen series of pseudoterpyridine Zn^{2+} complexes. *Acta Crystallogr B*. 2013;69(1):43-54.
54. Dumitru F, Legrand Y-M, Petit E, van der Lee A, Barboiu M. Self-sorting of metallosupramolecular DCLs via double-level exchange: amplification in solution and solid state modulation. *Dalton Trans*. 2012;41(38):11860-11865.
55. Dumitru F, Legrand Y-M, Barboiu M, Petit E, van der Lee A. Metallosupramolecular architectures of pseudoterpyridine-type ligands and Zn^{2+} metal ions. *Cryst Growth Des*. 2009;9(6):2917-2921.
56. Legrand Y-M, Dumitru F, van der Lee A, Barboiu M. Interpenetrated constitutional networks of aromatic metallosupramolecular duplexes. *Supramol Chem*. 2009;21(3-4):229-236.
57. Dumitru F, Petit E, van der Lee A, Barboiu M. Homo- and heteroduplex complexes containing terpyridine-type ligands and Zn^{2+}. *Eur J Inorg Chem*. 2005;21(9):4255-4262.
58. Vance AL, Alcock NW, Heppert JA, Busch DH. An octahedral template based on a new molecular turn: synthesis and structure of a model complex and a reactive, diphenolic ligand and its metal complexes. *Inorg Chem*. 1998;37(26):6912-6920.
59. CrysAlis^{Pro} Rigaku Oxford Diffraction Technologies, England 2012.
60. van der Lee A. Charge flipping for routine structure solution. *J Appl Cryst*. 2013;46:1306-1315.
61. Hooft RWW, Straver LH, Spek AL. Determination of absolute structure using Bayesian statistics on Bijvoet differences. *J Appl Cryst*. 2008;41(1):96-103.
62. Palatinus L, Chapuis G. *SUPERFLIP*—a computer program for the solution of crystal structures by charge flipping in arbitrary dimensions. *J Appl Cryst*. 2007;40(4):786-790.
63. Flack HD. On enantiomorph-polarity estimation. *Acta Crystallogr A*. 1983;39:876-881.
64. Flack HD, Bernardinelli G. Absolute structure and absolute configuration. *Acta Crystallogr A*. 1999;55:908-915.
65. Flack HD, Bernardinelli G. The use of X-ray crystallography to determine absolute configuration. *Chirality*. 2008;20(5):681-690.
66. Flack HD, Sadki M, Thompson AL, Watkin DJ. Practical applications of averages and differences of Friedel opposites. *Acta Crystallogr A*. 2011;67:21-34.
67. Parsons S, Flack HD, Wagner T. Use of intensity quotients and differences in absolute structure refinement. *Acta Crystallogr B*. 2013;69(3):249-259.
68. Betteridge PW, Carruthers JR, Cooper RI, Prout K, Watkin DJ. *CRYSTALS* version 12: software for guided crystal structure analysis. *J Appl Cryst*. 2003;36(6):1487-1487.
69. Cooper RI, Thompson AL, Watkin DJ. *CRYSTALS* enhancements: dealing with hydrogen atoms in refinement. *J Appl Cryst*. 2010;46:1100-1107.
70. Somogyi L, Samu E, Huszthy P, et al. Circular dichroism of host–guest complexes of achiral pyridino- and phenazino-18-crown-6 ligands with the enantiomers of chiral aralkyl ammonium salts. *Chirality*. 2001;13(2):109-117.
71. Donnoli MI, Giorgio E, Superchi S, Rosini C. Circular dichroism spectra and absolute configuration of some aryl methyl sulfoxides. *Org Biomol Chem*. 2003;1(19):3444-3449.
72. Llunell M, Casanova D, Cirera J, Alemany P, Alvarez S. *SHAPE: program for the stereochemical analysis of molecular fragments by means of continuous shape measures and associated tools, 2.1*. Barcelona: University of Barcelona; 2013.

73. Alvarez S. Distortion pathways of transition metal coordination polyhedra induced by chelating topology. *Chem Rev*. 2015;115 (24):13447-13483.

74. Janiak C. A critical account on π–π stacking in metal complexes with aromatic nitrogen-containing ligands. *J Chem Soc Dalton Trans*. 2000;21:3885-3896.

75. Langs DA. Three-dimensional structure at 0.86 A of the uncomplexed form of the transmembrane ion channel peptide gramicidin A. *Science*. 1988;241(4862):188-191.

76. Cohen C. Why fibrous proteins are romantic. *J Struct Biol*. 1998;122(1-2):3-16.

77. Creager AN. The Life of a Virus: Tobacco Mosaic Virus as an Experimental Model, University of Chicago Press, 2002.

SUPPORTING INFORMATION

Additional supporting information may be found online in the Supporting Information section at the end of the article.

How to cite this article: Dumitru F, van der Lee A, Barboiu M. Chiral superstructures from homochiral Zn^{2+}, Co^{2+}, Fe^{2+}-2,6-bis (*aryl* ethylimine)pyridine complexes. *Chirality*. 2019;1–13. https://doi.org/10.1002/chir.23115